Available online at www.sciencedirect.com
SCIENCE DIRECT®
Journal of Magnetism and Magnetic Materials 300 (2006) e8–e11
Journal of magnetism and magnetic materials
www.elsevier.com/locate/jmmm

Magnetic properties of CdSb doped with Ni

R. Laiho[a,*], A.V. Lashkul[a,b], E. Lähderanta[a,c], K.G. Lisunov[a,d], I. Ojala[a], V.S. Zakhvalinskii[a,e]

[a] *Wihuri Physical Laboratory, University of Turku, FIN-20014 Turku, Finland*
[b] *Faculty of Technology, University of Vaasa, FIN-65101 Vaasa, Finland*
[c] *Department of Physics, Lappeenranta University of Technology, FIN-53851 Lappeenranta, Finland*
[d] *Institute of Applied Physics, Academiei Street, 5, MD-2028 Kishinev, Moldova*
[e] *Department of Physics, Belgorod State University, RUS-308015 Belgorod, Russian Federation*

Available online 15 November 2005

Abstract

Magnetic properties of the group II–V semiconductor CdSb single crystals doped with Ni (2 at%) are investigated. Deviation of the zero-field-cooled susceptibility, χ_{ZFC}, from the field-cooled susceptibility is observed below 300 K, along with a broad maximum of $\chi_{ZFC}(T)$ at T_b in fields below the anisotropy field $B_K \sim 4$ kG. $T_b(B)$ obeys the law $[T_b(B)/T_b(0)]^{1/2} = 1 - B/B_K$ with $T_b(0) \sim 100$ K. The magnetization exhibits saturation above ~20–30 kG, a weak temperature dependence and anisotropy of the saturation value M_s. The coercive field is much smaller then B_K and displays anisotropy inverted with respect to that of M_s. Such magnetic behavior is expected for spheroidal Ni-rich $Ni_{1-x}Sb_x$ nanoparticles with high aspect ratio, broad distribution of the sizes and with orientations of the major axis distributed around a preferred direction.

PACS: 5.50. Pp; 75.50.Tt; 75.60. Jk

Keywords: Magnetic semiconductors; Anisotropy; Nanoparticles

1. Introduction

Cadmium antimonide, CdSb, has an orthorhombic crystal structure and strongly anisotropic transport properties, as typical of group II–V semiconductors [1]. Undoped CdSb is diamagnetic with values of the magnetic susceptibility, χ, depending on the crystallographic direction. Doping with different elements strongly influences transport and magnetic properties of CdSb [1]. With Ni an eutectic composition of CdSb + NiSb at ~2 mol% of NiSb is formed containing needle-like NiSb inclusions, with the length of the needles ~30–40 μm and the diameter ~1–1.5 μm, oriented preferably along the direction of growth of the ingot [2]. Therefore, at small doping levels of Ni the formation of nanosize spheroidal Ni-rich $Ni_{1-x}Sb_x$ clusters with a high aspect ratio can be expected. Because $Ni_{1-x}Sb_x$ is ferromagnetic at $x \leqslant 7.5\%$ [3], the system of Ni-rich nanoclusters is likely to exhibit interesting magnetic behavior.

In this work, we investigate magnetic properties of CdSb:Ni, giving evidence for the presence of the Ni-rich $Ni_{1-x}Sb_x$ nanoclusters and analyze their properties.

2. Results and discussion

Single crystals of CdSb doped with Ni (2 at%) were prepared with a modified Bridgman method [1]. The samples were cut in the form of rectangular prisms oriented along the crystalline directions [1 0 0], [0 1 0] and [0 0 1]. DC magnetization, M, was measured with a SQUID magnetometer in a field, B, parallel to one of the crystallographic axes, after cooling the sample in zero-field (ZFC) or in a field (FC). Thermoremanent magnetization (TRM) was measured after cooling the sample from the room temperature down to 5 K in a magnetic field and then reducing the field to zero.

*Corresponding author. Tel.: +1 358 2 3335 943; fax: +1 358 2 2319636.
E-mail address: reino.laiho@utu.fi (R. Laiho).

0304-8853/$ - see front matter © 2005 Elsevier B.V. All rights reserved.
doi:10.1016/j.jmmm.2005.10.137

As can be seen from Fig. 1, after subtraction of the diamagnetic background a clear deviation of the plots of $\chi_{ZFC}(T)$ and $\chi_{FC}(T)$ is observed below 300 K. In addition, $\chi_{ZFC}(T)$ has a broad maximum around $T_b \sim 100$ K in the lowest applied field. The magnetic irreversibility is suppressed with increasing the field and vanishes above 4 kG, whereas T_b is shifted to a lower temperature. In the bottom panel of Fig. 1 a large difference between the plots of TRM(T) and $\chi_{FC}(T)$–$\chi_{ZFC}(T)$ can be seen.

The field dependence of magnetization exhibits saturation already above ~20–30 kG. The saturation magnetization $M_s^{(j)}$ along the jth axis ($j = 1$, 2 and 3 for B||[1 0 0], [0 1 0] and [0 0 1], respectively) in the bottom panel of Fig. 2

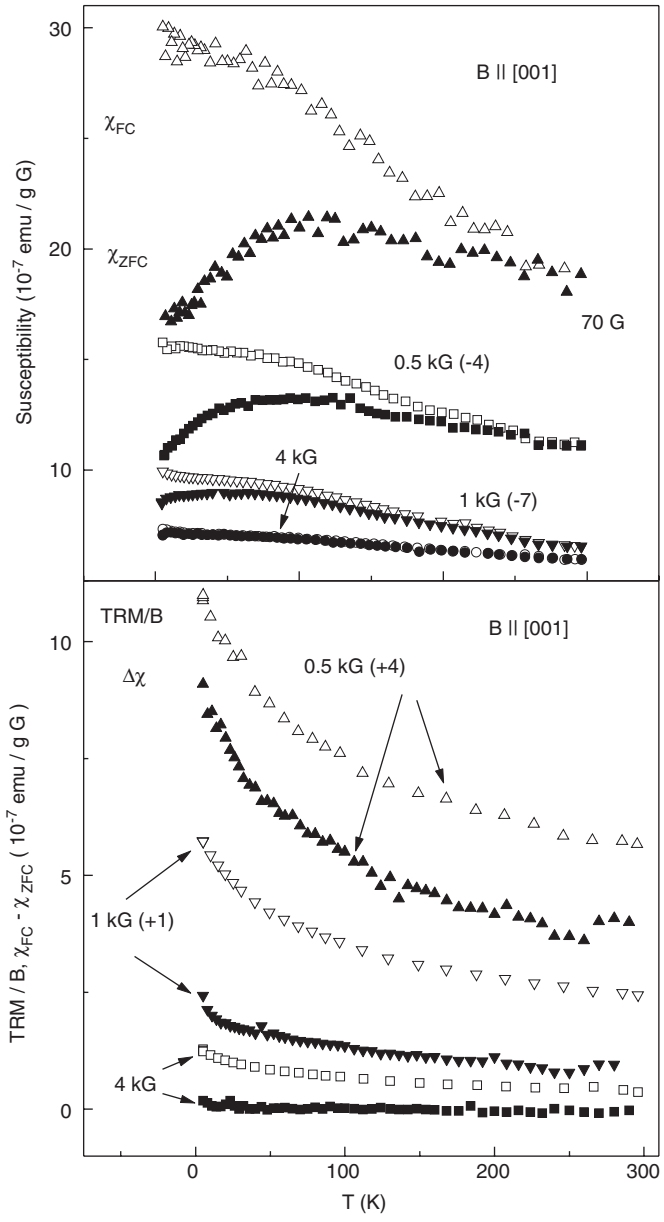

Fig. 1. Upper panel: χ_{FC} (open symbols) and χ_{ZFC} (closed symbols) vs. T. Lower panel: TRM /B (open symbols) and $\Delta\chi = \chi_{FC} - \chi_{ZFC}$ (closed symbols) vs. T. Some of the curves are shifted along the vertical axes by the values shown in parenthesis (in 10^{-7} emu/g G).

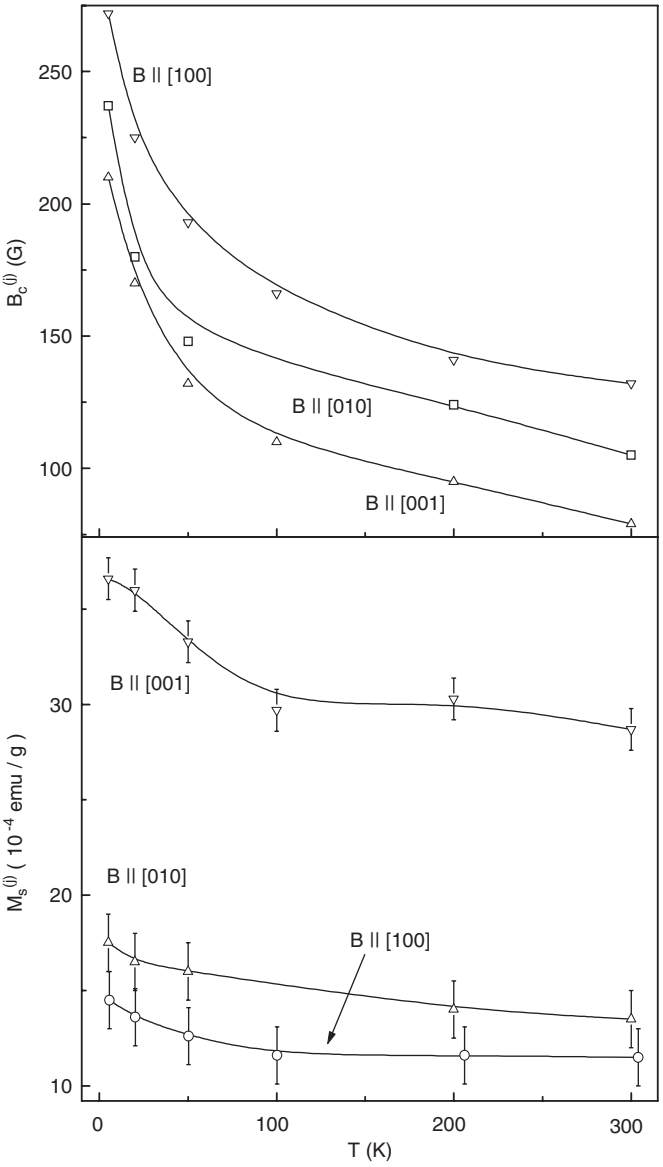

Fig. 2. Upper panel: temperature dependence of $B_c^{(j)}$. Lower panel: temperature dependence of $M_s^{(j)}$. The lines are to guide the eye.

displays a weak temperature dependence (increasing below ~100 K) and the relation of $M_s^{(1)} < M_s^{(2)} < M_s^{(3)}$ (the scattering of the data points is due to subtraction of the diamagnetic contribution). The hysteresis is characterized by temperature dependence of the coercive field, $B_c^{(j)}$, which is enhanced below ~100 K (see Fig. 2). The coercive field exhibits anisotropy, which is inverted with respect to that of $M_s^{(j)}$.

The magnetic properties above give evidence for the existence of nanosize Ni-rich magnetic particles in the samples. Because at high doping levels of Ni, the NiSb needles are segregated in the CdSb host, at a doping level as low as 2 at% the nanoparticles are expected to contain a $Ni_{1-x}Sb_x$ phase with $x < 7$ at%, having the Curie temperature $T_C > 300$ K [3]. Therefore, the deviation of $\chi_{ZFC}(T)$ from $\chi_{FC}(T)$ and the maximum of $\chi_{ZFC}(T)$ at T_b (Fig. 1)

are attributable to blocking of the moments of the $Ni_{1-x}Sb_x$ clusters due to the anisotropy energy barriers $\sim KV$, where K is the density of the anisotropy energy and V is the volume of the particle. It can be seen that $T_b \approx KV/(25k)$ depends strongly on the size of the particles. Therefore, the broadness of the maximum and the large difference between the values of $T_b \sim 100$ K and the onset temperature of the magnetic irreversibility ~ 300 K in a low field, can be explained by a broad distribution of the sizes of the clusters (Fig. 1). The applied magnetic field reduces the anisotropy energy barriers leading to decrease of T_b according to the relation $[T_b(B)/T_b(0)]^{1/2} \approx 1-B/B_K$, where B_K is the mean anisotropy field [4]. As can be seen in Fig. 3 the field dependence of T_b is close to this relation, giving $T_b(0) = 107 \pm 5$, 105 ± 5, 110 ± 3 K and $B_K = 3.9 \pm 0.5$, 4.7 ± 0.5 and 4.5 ± 0.5 kG for B parallel to [1 0 0], [0 1 0] and [0 0 1], respectively. As $B \to B_K$ the magnetic irreversibility decreases and vanishes for $B \sim B_K$, which explains the damping of the difference between $\chi_{ZFC}(T)$ and $\chi_{FC}(T)$ in Fig. 1, and yields the values of $B_K \sim 4$ kG, similar with those obtained above. With the equation $B_K/T_b(0) \approx 50\, k_B/\mu$ [4], we obtain the cluster moment $\mu = (2.0 \pm 0.2) \times 10^4$, $(1.7 \pm 0.2) \times 10^4$ and $(1.8 \pm 0.2) \times 10^4 \mu_B$ for B parallel to [1 0 0], [0 1 0] and [0 0 1], respectively.

For an assembly of spherical clusters the relation TRM $(T) \approx M_{FC}(T) - M_{ZFC}(T)$ is expected to be fulfilled, while deviations from this relation are associated with the shape anisotropy of the clusters [5]. Hence, the large difference between $TRM(T)/B$ and $\chi_{FC}(T) - \chi_{ZFC}(T)$ (Fig. 1) is attributable to a considerable non-sphericity of the Ni-rich clusters.

The picture above is valid without restrictions only for an assembly of *single-domain particles* and the magnetization reversal process by *coherent rotation*. This is fulfilled for $r << r_{sd}$ and $r << r_c$, where r is the radius of the particles. The critical radii of the single-domain particle, r_{sd}, and of the coherent rotation, r_c, satisfy the equations $(N_c/6A)(M_s^*)^2 r_{sd}^2 = \ln(4r_{sd}/a)$-1 and $r_c = q(2/N_a)^{1/2} A^{1/2}/M_s^*$, respectively. Here M_s^*, a and A are the saturation magnetization, the distance between the magnetic ions and the exchange stiffness constant of the cluster material, respectively, and $N_a(m)$ is the demagnetization factor of the cluster. For a spheroidal particle the factors $N_c(m)$ and $N_a(m)$ refer to its major and minor axes, respectively, and $m = l/r$ is the aspect ratio, where l is the semi-length of the major axis [6]. However, it can be shown that the relation of $B_c^{(j)}(T) < < B_K$, *observed for any direction of the field*, contradicts the coherent rotation [6]. The magnetization reversal mode can be determined from temperature dependence of the coercivity, which for an assembly of blocked single-domain nanoparticles with narrow size distribution is given by the law $B_c^{(j)}(T) = B_c^{(j)}(0)\{1-[T/T_b(0)]^n\}$, where $n = 1/2$ and $2/3$ for the magnetization reversal by coherent rotation and by *curling* (which is valid for $r_c << r << r_{sd}$), respectively [7]. However, neither value of n can be adjusted to fit our coercivity data in Fig. 2, excluding an interval between ~ 5 and 20 K which is too narrow to determine the magnetization reversal mode unambiguously. This is attributable to a broad size distribution of the clusters as evident from Fig. 1. Nevertheless, it can be shown that the anisotropy of coercivity and saturation magnetization give evidence for the magnetization reversal by curling. The origin of anisotropy suggests, besides the sufficiently high aspect ratio, the non-random orientations of the cluster spheroids distributed around the preferred direction. At an initial approximation the scattering of the angles θ_j between the major axis of the spheroid (parallel to the zero-temperature magnetization $M_s^{(j)}(0)$ for high m) and jth crystallographic axis can be neglected, leading to an equation ($j = 1$, 2 and 3)

$$B_c^{(j)}(0) = 2\pi M_s^* [XY/(X \sin^2(\theta_j) + Y \cos^2(\theta_j)]^{1/2}, \quad (1)$$

where $X = (2D_c - \kappa/S^2)^2$, $Y = (2D_a - \kappa/S^2)^2$, $D_a = N_a/(4\pi)$, $D_c = N_c/(4\pi)$, $S = r/r_0$, $r_0 = A^{1/2}/M_s^*$ and κ depends weakly on m ($\kappa = 1.08-1.38$ for $1 \leqslant m < \infty$) [6]. In the same approximation we can write

$$M_s^{(j)}(0) = \eta M_s^* [1 - D(\theta_j)] \cos(\theta_j), \quad (2)$$

where η is the volume fraction of the $Ni_{1-x}Sb_x$ phase and $D(\theta_j) = D_a \sin^2\theta_j + D_c \cos^2\theta_j$. It can be shown that for $m \geqslant 4$ and for reasonable cluster parameters the relation of $X << Y$ is valid, which allows exclusion of M_s^* from Eq. (1) by taking ratios of $B_c^{(i)}(0)/B_c^{(k)}$ (0), $i \neq k$. Together with the constraint equation $\cos^2(\theta_1) + \cos^2(\theta_2) + \cos^2(\theta_3) = 1$ this gives a closed system of equations for θ_j, yielding $\theta_j^{(B)} = 60^\circ$, 54° and 49° (the label 'B' means that the angles are determined from the coercive field data, extrapolated to $T = 0$) for $j = 1$, 2 and 3, respectively. In a similar way, we find the values obtained from the magnetization data, $\theta_j^{(M)} = 66^\circ$, 62° and 39° for $j = 1$, 2 and 3, respectively, where for $M_s^{(j)}(0)$ we take the values of $M_s^{(j)}$ in the interval of the weak variation in Fig. 2. It is evident that both sets

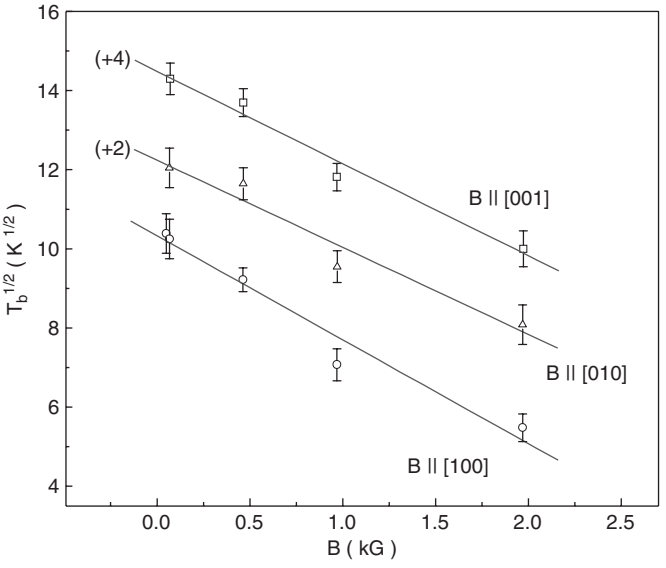

Fig. 3. Dependence of $T_b^{1/2}$ on B. The lines are linear fits. Two plots are shifted along the vertical axis by the values shown in parenthesis (in $K^{1/2}$).

of angles $\theta_j^{(B)}$ and $\theta_j^{(M)}$ satisfy the same relation of $\theta_1 > \theta_2 > \theta_3$ *despite of the mutually inverted anisotropy* of $M_s^{(j)}$ and $B_c^{(j)}$ (Fig. 2). It can also be shown that the differences of ~10–20% between $\theta_j^{(B)}$ and $\theta_j^{(M)}$ are connected to a small distribution of the orientations of the clusters around the mean values.

At reasonable values of M_s^* (between 200–500 emu/cm^3 [3]) and m~4–8 we can estimate r~3.6–2.6 nm, r_c~2.5–1.2 nm and r_{sd}~120–160 nm, giving evidence for a strictly single-domain regime ($r << r_{sd}$). However, the values of r and r_c are comparable, which leads to a wide crossover interval between the coherent rotation and curling modes, due to a broad distribution of the sizes of the clusters evident from the discussion above. This explains the features of the magnetic behavior of our system, typical of both magnetization reversal processes—the magnetic irreversibility and dependence of $T_b(B)$ pertinent to coherent rotation, and the anisotropies of $M_s^{(j)}$ and $B_c^{(j)}$ characteristic of curling.

To summarize, we have investigated magnetization of CdSb doped with 2 at% of Ni. The observed magnetic properties give evidence for the presence of Ni–rich $Ni_{1-x}Sb_x$ spheroidal magnetic nanoclusters with a high aspect ratio and orientations, distributed around a preferred direction.

References

[1] E.K. Arushanov, Prog. Cryst. Growth Charact. 13 (1986) 1.
[2] S.F. Marenkin, M. Saidullaeva, V.P. Sanygin, I.S. Kovaleva, Izv. Acad. Nauk SSSR Neorg. Mater. 18 (1982) 1759.
[3] E. Kneller, Ferromagnetismus, Springer, Berlin, 1962.
[4] E.P. Wohlfarth, J. Phys. F 10 (1980) L241.
[5] N. Belous, I. Zorin, N. Kulich, I. Lezhnenko, A. Tovstolytkin, Sov. Phys. Solid State 32 (1990) 887.
[6] L. Sun, Y. Hao, C.L. Chien, P.C. Searson, IBM J. Res. Dev. 49 (2005) 79.
[7] H.Q. Yin, W.D. Doyle, J. Appl. Phys. 91 (2002) 7709.